

## PAPER

[View Article Online](#)  
[View Journal](#) | [View Issue](#)Cite this: *J. Mater. Chem. A*, 2025, **13**, 23928**[2 + 2] light-driven cycloaddition synthesis of an organic polymer and photocatalytic activity enhancement *via* monomer truncation†**Giacomo De Crescenzo,<sup>ID a</sup> Beatriz de Santos,<sup>ID a</sup> M. José Capitán,<sup>ID bc</sup> Jesús Álvarez,<sup>ID bdef</sup> Silvia Cabrera,<sup>ID gh</sup> Alberto Fraile,<sup>ID \*ah</sup> Matías Blanco<sup>ID \*ah</sup> and José Alemán<sup>ID \*ahi</sup>

The synthesis of covalent organic polymers usually relies on polar reactions for the establishment of linkages among the constituent monomers. Herein, the photochemical [2 + 2] olefin cycloaddition reaction is employed as a polymerization tool to yield organic polymers in which the connectivity is based on cyclobutane moieties, as demonstrated by the characterization techniques. The functionalization of the polymer is carried out by means of the monomer truncation strategy with monotopic olefins decorated with different motifs, including the organic photocatalyst 10-phenyl-phenothiazine (PTH), achieving its connection with a homogeneous 10% functionalization degree. All materials are active photocatalysts in the light-driven oxidative coupling of benzyl amines to the corresponding imines, but the functionalized polymer bearing a photoactive moiety shows an enhancement of the catalytic performance. Indeed, the functionalized-PTH polymer exhibits higher activity (75% yield vs. ~40% yield) and a stable recyclable character without leaching compared to the non-truncated sample.

Received 20th March 2025

Accepted 14th June 2025

DOI: 10.1039/d5ta02288f

[rsc.li/materials-a](https://rsc.li/materials-a)**Introduction**

Covalent organic polymers are a broad class of materials able to form 2D or 3D networks whose building blocks feature light elements such as C, H, N, O, S and/or B. As such, they differ from metal–organic frameworks in the absence of metals and in their connectivity.<sup>1–3</sup> Notably, this family of organic materials presents desirable characteristics such as synthesis by design, leading to tuneable structures with controllable pore dimension

and volume, as well as good mechanical strength, biocompatibility and semiconducting behaviour among others.<sup>4</sup> Thus, they are finding application in a great variety of fields, such as optoelectronic devices, (bio)sensors, composite crafting, gas and liquid separation, energy-related purposes or (photo) catalysis.<sup>5–15</sup>

Fundamentally, the choice of linker is paramount for the design of these materials. In this sense, the functional groups present in the polytopic monomers react in a controlled manner to form extended networks.<sup>16,17</sup> The synthesis of the materials often relies on classic thermally activated reactions; reversible reactions, such as condensations, usually yield materials with high crystallinity and porosity, while irreversible processes often produce more amorphous samples.<sup>18,19</sup> However, it would be highly desirable to develop sustainable methodologies to synthesize novel organic materials. Among these, photochemistry has lately attracted widespread attention for restoring the traditional classic systems in organic chemistry due to its sustainability and availability of light sources.<sup>20–23</sup> Nevertheless, photochemistry is nowadays scarcely applied as a synthetic tool for the development of organic materials, in part due to the difficult scalability of the methodology as well as the irreversibility of most photochemical processes. Few examples are reported in the literature, in which post-synthetic modifications over materials are performed through the use of photocatalytic methods. Very recently, light has been employed for the transformation of covalent organic frameworks synthesized *via*

<sup>a</sup>Organic Chemistry Department, Universidad Autónoma de Madrid, 28049 Madrid, Spain. E-mail: [alberto.fraile@uam.es](mailto:alberto.fraile@uam.es); [matias.blanco@uam.es](mailto:matias.blanco@uam.es); [jose.aleman@uam.es](mailto:jose.aleman@uam.es)

<sup>b</sup>Física de Sistemas Crecidos con Baja Dimensionalidad, Universidad Autónoma de Madrid, Unidad Asociada al CSIC por el IEM, 28049 Madrid, Spain

<sup>c</sup>Instituto de Estructura de la Materia IEM-CSIC, 28006-Madrid, Spain

<sup>d</sup>Instituto de Ciencia de Materiales “Nicolás Cabrera”, Universidad Autónoma de Madrid, 28049-Madrid, Spain

<sup>e</sup>Instituto de Física de la Materia Condensada IFIMAC, Universidad Autónoma de Madrid, 28049-Madrid, Spain

<sup>f</sup>Condensed Matter Physics Department, Universidad Autónoma de Madrid, 28049 Madrid, Spain

<sup>g</sup>Inorganic Chemistry Department, Universidad Autónoma de Madrid, 28049 Madrid, Spain

<sup>h</sup>Institute for Advanced Research in Chemical Sciences (IAdChem), Universidad Autónoma de Madrid, 28049 Madrid, Spain

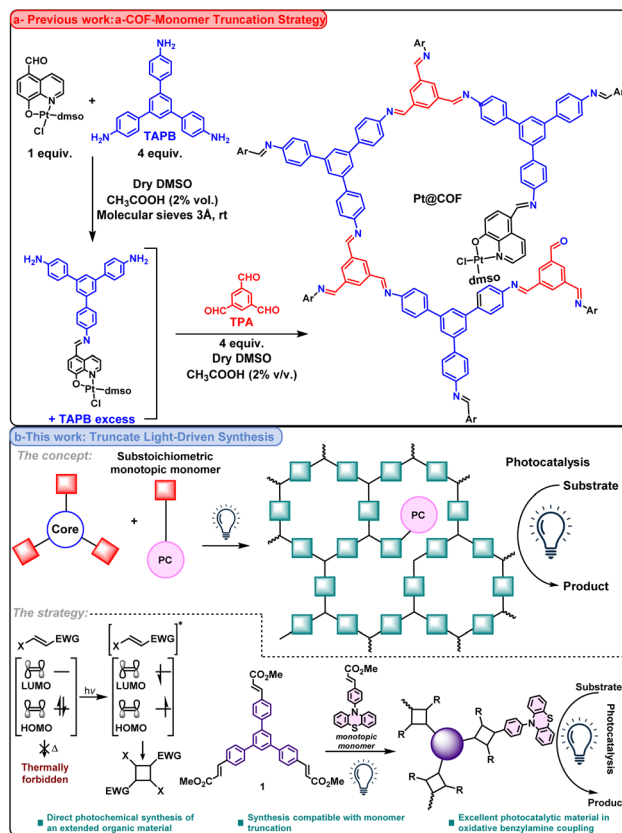
<sup>i</sup>Center for Innovation in Advanced Chemistry (ORFEO-CINQA), Universidad Autónoma de Madrid, 28049 Madrid, Spain

† Electronic supplementary information (ESI) available. See DOI: [10.1039/d5ta02288f](https://doi.org/10.1039/d5ta02288f)

thermally activated Schiff-base condensation with three different approaches (Scheme 1).<sup>24–26</sup> On the one hand, a multi-component process involving a photocatalytic Petasis reaction has been employed for the synthesis of a highly modified covalent organic framework. Light is employed as a post-modification tool as the Petasis reaction occurs between a trifluoroborate salt and the already *in situ* preformed hydrazone–azine structure (Scheme 1a).<sup>24</sup> Another approach implies the synthesis of a benzoxazole-linked covalent organic framework *via* light-driven cyclization of the polymer resulted from the Schiff-base condensation of polytopic aldehydes and *o*-hydroxyanilines (Scheme 1b).<sup>25</sup> Very recently, another material has been reported exploiting an iridium photocatalyst to promote a Povarov reaction over an imine-linked preformed structure. This strategy yielded a covalent organic framework in which the monomers are linked through quinoline units (Scheme 1c).<sup>26</sup> All these examples present the construction of complex structures by sequential polar-photochemical transformations; however, it would be of great significance to obtain an organic material using only photochemistry or photocatalysis as a synthetic tool.

In this regard, [2 + 2] photocycloaddition can be a viable and promising strategy to generate an organic material through light-driven polymerization. This reaction is a pericyclic transformation that simultaneously creates two  $\sigma$ -bonds from two olefins which upon light irradiation generate cyclobutanes.<sup>27,28</sup> This reactivity is forbidden under thermal activation due to the relative antibonding approach of the HOMO and LUMO of both  $\pi$  systems. However this pericyclic reaction proceeds through the light-promoted excitation of one electron from the  $\pi$  to the  $\pi^*$  orbital of one of the reacting olefins, thus reaching a situation in which the symmetry requirements for orbital overlapping are fulfilled (bottom left, Scheme 2b).<sup>29</sup> This photocycloaddition has been previously employed as a tool for modification of polymers, or to promote on-surface and/or solid-state polymerizations;<sup>30,31</sup> nevertheless, to the best of our knowledge, examples for creating a polymer in solution under light-driven [2 + 2] cycloadditions are still unexplored.

Our research group has recently reported the incorporation of a photocatalytically active platinum complex into an imine



Scheme 2 (a) Previous work of our group related to monomer truncation under thermal conditions. (b) Concept and strategy of [2 + 2] polymerization, including the monomer truncation strategy performed in this work.

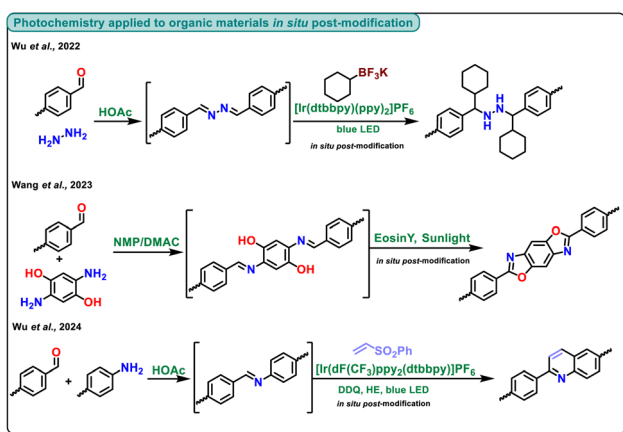
covalent organic framework *via* the monomer truncation strategy (Scheme 2a),<sup>32</sup> which entails the introduction of substoichiometric amounts of monotopic monomers which interrupt the network resulting in a random distribution of structural defects along the COF backbone. This strategy allows us to enhance the functionality of the material,<sup>33</sup> and has been employed for photocatalytic purposes.<sup>32,34</sup>

Therefore, in this work we present the synthesis of a cyclobutane-linked organic material employing a photochemical [2 + 2] cycloaddition between polytopic olefins. This approach yields an amorphous polymer with  $\mu$ m-sized laminar aggregates and semiconducting character. Furthermore, we combined light-driven polymerization with the monomer truncation strategy,<sup>33</sup> which allows us to expand the functionality of the polymer, especially through the inclusion of an organic photocatalyst. Integrating these two methodologies, we used light to produce a novel material and as an energy source to promote photocatalytic reactions (bottom, Scheme 2b).

## Results and discussion

### Synthesis of the materials and characterization

We started our study with the synthesis of the building blocks and truncating units required for the polymer's assembly (see



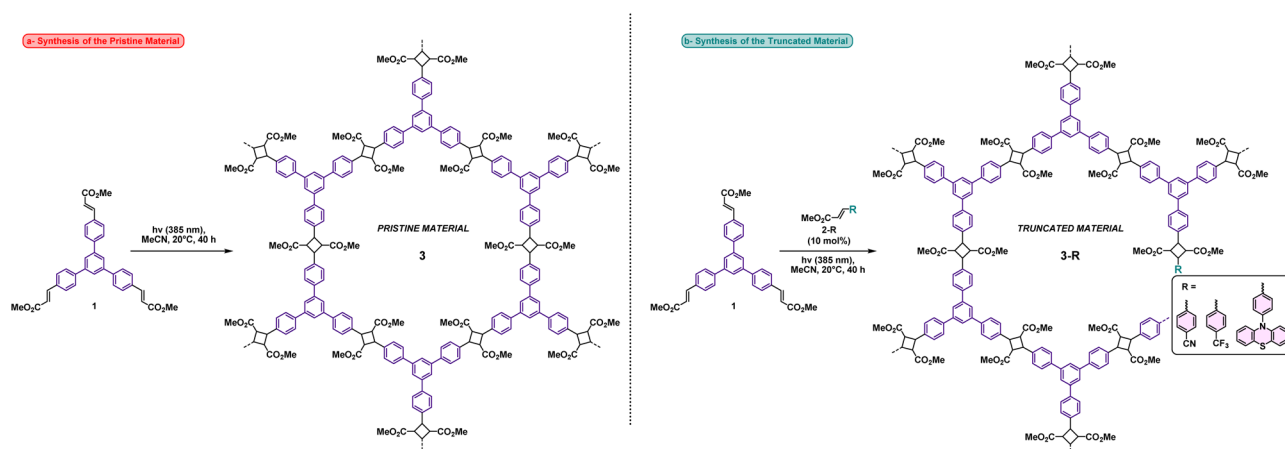
Scheme 1 Current photochemical transformations applied to extended organic material synthesis *in situ* post-modification.



the ESI† for full details on the synthesis and characterization of the molecules). On the one hand, the synthesis of trimethyl 4,4',4''-benzene-1,3,5-triyl-tricinnamate (**1**) was achieved *via* a Heck-type reaction between 1,3,5-tris(*p*-bromophenyl)benzene and methyl acrylate in 70% yield (Scheme S1 in the ESI†).<sup>35</sup> On the other hand, the synthesis of methyl *p*-cyano-*trans*-cinnamate (**2-CN**, 97% yield) and methyl *p*-trifluoromethyl-*trans*-cinnamate (**2-CF<sub>3</sub>**, 81% yield) was accomplished by Fischer esterification from the corresponding cinnamic acids (Scheme S2 and S3 in the ESI†),<sup>36</sup> while the methyl acrylate of 10-phenylphenothiazine (**2-PTH**) could be generated *via* a Buchwald-Hartwig coupling between phenothiazine and methyl *p*-bromo-*trans*-cinnamate in 60% yield (Scheme S4 in the ESI†).<sup>37</sup>

When monomer **1** was subjected to an intermolecular [2 + 2] photocycloaddition with itself, the organic polymer **3** was yielded as a pale-yellow solid, where the monomers are connected to each other *via* the new cyclobutane moieties created (Scheme 3a) (see the ESI† for full details on the synthesis). According to the light absorption properties of monomer **1** (Fig. S16 at ESI†), the [2 + 2] photocycloaddition should not require the presence of an additional photocatalyst to promote the excitation of the  $\pi$  electrons if the polymerization is conducted under 385 nm LED irradiation. The reaction time (40 h) was selected according to the disappearance of the free monomer in the supernatant as tracked by liquid <sup>1</sup>H NMR and the disappearance of the olefinic C=C stretching band in the FTIR spectrum of the yielded material (see below). In order to introduce more functionality in the final material, light-driven [2 + 2] polymerization cycloaddition was performed in the presence of a sub-stoichiometric amount (10 mol%) of the mono-alkenes **2-R** (Scheme 3b). In this way, the light-driven monomer truncation polymerizations provided different materials that contain a defective node with the target functionality,<sup>33,34</sup> *i.e.*, a benzonitrile for material **3-CN** and a trifluoromethyl moiety in sample **3-CF<sub>3</sub>**, while **3-PTH** contains the 10-phenyl phenothiazine photoactive molecule.<sup>26,38</sup> For comparative purposes, monomer **2-PTH** was also subjected to a [2 + 2] photocycloaddition with itself to yield molecule **2-cb** to be used as a homogeneous reference (see Scheme S5 in the ESI† for further details).

The photosynthesized polymers were characterized by means of typical solid characterization techniques. On the one hand, Cross Polarization combined to Magic Angle Spinning <sup>13</sup>C solid state Nuclear Magnetic Resonance (<sup>13</sup>C-ss-CPMAS-NMR) revealed both aromatic and aliphatic features for all samples, in accordance with the expected structure (see left-Figure 1). In particular, **3** presents a broad aromatic region corresponding to the benzene rings present in the building blocks. In addition, the carbon atom for the ester group could be also observed at 172.4 ppm, as observed by comparison with the respective spectral features of the monomers and dimer (see Fig. 1 and the ESI†); furthermore, the aliphatic region shows a signal at 51.3 ppm which corresponds to the methyl carbon at the ester group, and another broad signal centered at 44.1 ppm, which can be assigned to the new cyclobutane core created. It is worth mentioning that the signals corresponding to the double bonds (at 116 and 145 ppm for monomers **1** and **2**) were not observed in the NMR spectrum of any samples,<sup>39</sup> which is indicative of a successful polymerization reaction. Nevertheless, the substoichiometric and low loading of the truncating agents employed in the synthesis of materials **3-R**, combined with the signals overlapping due to the great number of aromatic carbons, did not permit distinguishing the signals arising from the truncating moieties in the aromatic region. The comparison of previous <sup>13</sup>C-NMR data with those obtained for homogeneous **2-cb**, especially in the aliphatic region, confirms that the [2 + 2] photocycloaddition polymerization has taken place correctly. Furthermore, a sharp CF<sub>3</sub> peak could be observed at -63 ppm in the corresponding solid state <sup>19</sup>F-NMR spectrum of sample **3-CF<sub>3</sub>** (see Fig. S3 in the ESI†). Additionally, Fourier Transformed InfraRed (FTIR) spectroscopy was used to cross-check the NMR data (see right Fig. 1). Indeed, the most upshifted signal in the spectrum of sample **3** appeared at 2950 cm<sup>-1</sup>, indicative of both the CH<sub>3</sub> and aliphatic C-H vibrations. Then, the stretching of ester groups and the aromatic cores merged at 1740 and 1590 cm<sup>-1</sup> of wavenumbers, respectively. A scissoring vibration at 1510 and 1455 cm<sup>-1</sup> may be ascribed to the cyclobutane moiety, according to previous reports and the comparison with the **2-cb** sample spectrum.<sup>40</sup>



Scheme 3 Synthesis of the polymers **3** (eqn (a)) and **3-R** (eqn (b)) *via* the [2 + 2] photocycloaddition reaction.



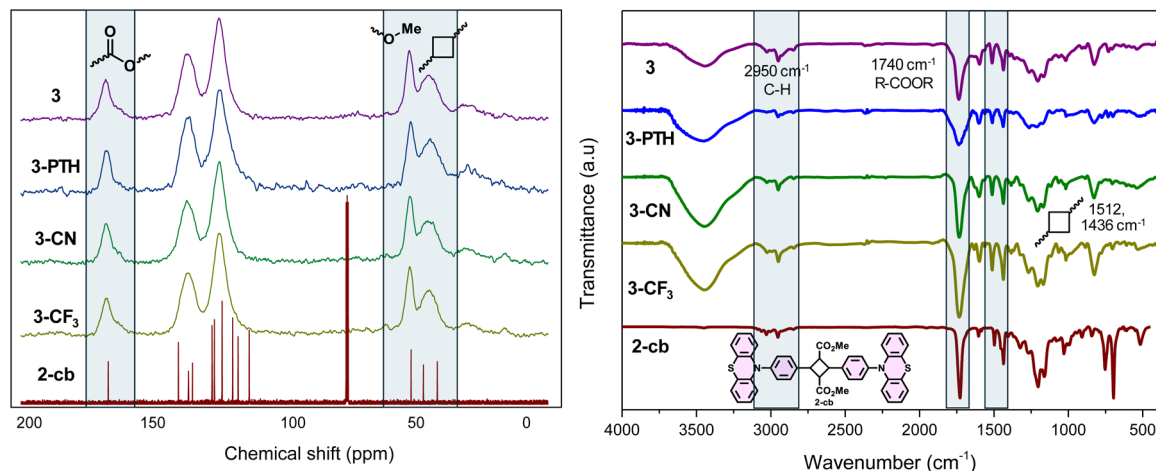


Fig. 1 Left:  $^{13}\text{C}$ -SS-CPMAS-NMR spectra of samples **3** (purple), **3-PTH** (blue), **3-CN** (green) and **3-CF<sub>3</sub>** (yellow) compared to the homogeneous **2-cb** (red) liquid  $^{13}\text{C}$ -NMR spectrum (in  $\text{CDCl}_3$ ); right: FTIR spectra of sample **3** (purple), **3-PTH** (blue), **3-CN** (green), **3-CF<sub>3</sub>** (yellow) and **2-cb** (red).

Meanwhile, the truncated polymers presented all the ascribed features found in the pristine material, as well as the more complex fingerprint region, probably arising from the truncation. In particular, the nitrile present in monomer **2-CN** exhibited a sharp peak at  $2228\text{ cm}^{-1}$  in the corresponding FTIR spectrum (see Fig. S3 in the ESI†).<sup>41</sup> This represents a strong demonstration of a successful monomer truncation strategy, indicating that the procedure is compatible with the light-driven  $[2 + 2]$  photocycloaddition polymerization.

The morphology of all materials was analyzed by means of Scanning Electron Microscopy (SEM). In general, all polymers appeared as amorphous to laminar aggregations with a mean particle size of  $30\text{--}50\text{ }\mu\text{m}$  (Fig. 2). Some depth was observed in these aggrupations, indicating a more complex packaging due to the stacking caused by eventual  $\pi$  interactions among the aromatic polymer core; conversely, other particles showed a more amorphous appearance. However, smooth surfaces were spotted for both types of morphologies, indicating high cohesion among particles since the extended organic polymer is

strongly connected by covalent bonds. Interestingly, more amorphous grouping and smaller mean sizes were detected for all the truncated samples, maybe due to the introduction of structural defects as a result of the monomer truncation, but the general morphology of the polymer **3** structure is mainly maintained.<sup>33</sup> The observed morphology is a result of the conditions employed in the polymerization and the type of bond created among the monomers since the steric requirements of the connecting cyclobutane ring might prevent a more ordered disposition of the polymer sheets.<sup>42</sup> Indeed, all samples present an amorphous character as shown by the powder X-ray diffraction patterns, where a very broad peak was observed between  $10^\circ$  and  $30^\circ$  of  $2\theta$  (see at Fig. S6–S9 in the ESI†). In addition, low porosity values of about  $7\text{ m}^2\text{ g}^{-1}$  of surface area was found for samples **3** and **3-PTH** (Fig. S10 at ESI†).

The local analysis employing an *in situ* EDX microprobe (Fig. S4 and S5 in the ESI†) revealed that the composition of the photopolymerized samples contained the characteristic elements of the introduced moieties homogeneously distributed all over the particles. For instance, sample **3** as expected only contained C and O (see Fig. S5 in the ESI†). Interestingly, the heteroatoms of the truncated defects could also be distinguished. First, sample **3-CN** presented signals associated with N due to the introduction of the nitrile group (see Fig. S5 in the ESI†). The same phenomenon was observed for sample **3-CF<sub>3</sub>**, which showed the presence of C, O and F atoms in the analyzed particles (see Fig. S5 in the ESI†). Finally, **3-PTH** contained C and O, as well as N and S signals. The presence of these atoms indicates that the functionalization with the monotopic olefins using the monomer truncation strategy had been performed successfully in all cases. The degree of functionalization could be averaged by elemental analysis for the bulk samples (Table 1). Polymer **3** presented a high C level of 75% as a result of the C content of the organic monomer, with negligible levels of N and S. Regarding the truncated materials, elemental analysis detected C-based polymers with increased amounts of heteroatoms (since F cannot be detected by this method, sample **3-CF<sub>3</sub>**

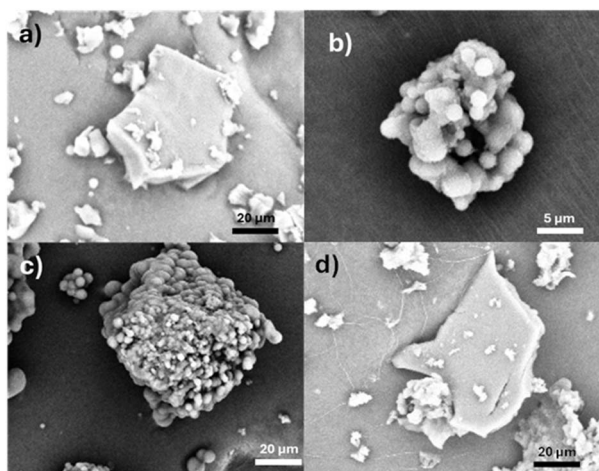


Fig. 2 SEM analysis of samples (a) **3**, (b) **3-CN**, (c) **3-CF<sub>3</sub>** and (d) **3-PTH**.





Table 1 Elemental analysis of the samples under study<sup>a</sup>

Sample	C [% wt]	H [% wt]	N [% wt]	S [% wt]
3	75.2	4.8	0.1	0.0
3-CN	71.8	5.5	1.0	0.0
3-PTH	73.1	5.4	0.8	0.9
3-PTH <sup>b</sup>	72.8	5.6	0.8	1.0

<sup>a</sup> All values are expressed in %wt. <sup>b</sup> Sample prepared with 25 mol% of 2-PTH.

was not subjected to elemental analysis). In particular, sample 3-CN showed 1.0% of N due to the truncated nitrile group, assuming an 8 mol% functionalization degree, in sharp agreement with the amount of truncating monomer added. In addition, the amount in sample 3-PTH was also increased up to 0.8% of N and 0.9% of S, which implies a 10 mol% functionalization degree. Interestingly, a sample prepared using a 25 mol% loading of the monotopic monomer 2-PTH afforded similar results in terms of N and S contents, which may indicate that the monomer truncation under [2 + 2] photocycloaddition conditions was limited to 10 mol% of the truncating monomer.

Keeping in mind the potential photocatalytic application, we carried out X-ray Photoelectron Spectroscopy (XPS) on pristine material 3 and the truncated sample decorated with the photoactive moiety 3-PTH. Indeed, the survey spectrum of both samples presented the characteristic XPS C 1s (285 eV of binding energy (BE)) and O 1s (BE of 533 eV) core level regions, while sample 3-PTH presented two peaks corresponding to XPS N 1s (BE of 399 eV) and S 2p (BE of 165 eV) core level regions as a result of the monomer truncation (see Fig. S11 in the ESI†). Therefore, this survey analysis cross-checked that the monotopic monomer 2-PTH has been introduced into the structure of the polymer. By analysing the components (Fig. 3a), the fit of the XPS C 1s core level region afforded two main components for sample 3, which may be assigned as a mixture contribution of C sp<sup>2</sup> and C sp<sup>3</sup> at lower BE (BE of 284.5 eV, dark cyan peak) and C bonded to heteroatoms at higher BE, which belongs to O in the case of sample 3 (286 of BE, pink peak). In addition, the interaction of the material with the Ag employed for sample set-up could not be avoided because a small peak at a BE of 282.6 eV (golden colour peak) was also extracted from the fit. Interestingly, sample 3-PTH presented broader signals as a result of the disorder introduced during the monomer truncation (Fig. 3b).<sup>33</sup> Indeed, the C–C peak at a BE of 284.5 eV got wider and overlapped the defect region, hindering the possibility of detecting new components such as C–N and C–S bonds. However, the different electronic distribution of the truncated material compared to sample 3 (see below) permits distinguishing the ester groups as a new peak obtained at a BE of 288 eV (navy peak) and assigned to C=O bonds.<sup>43</sup> Interestingly, the N 1s XPS core level signal could only be fitted with one corresponding component in agreement with the functionalizing unit introduced (pyridinic-like N),<sup>37</sup> being very close to the 10 mol% used for light-driven polymerization (Fig. 3c). However, the low S amount detected, lying close to the technique detection limit,

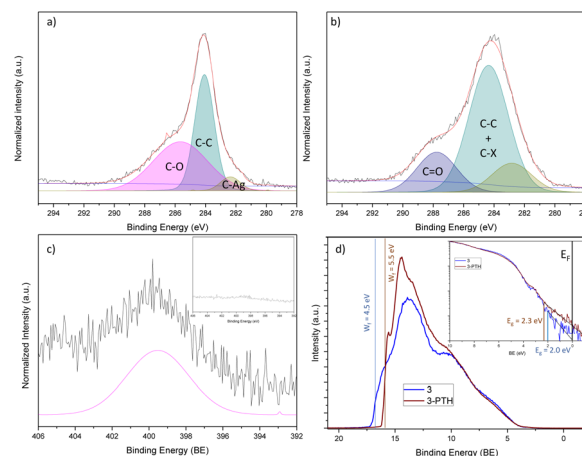
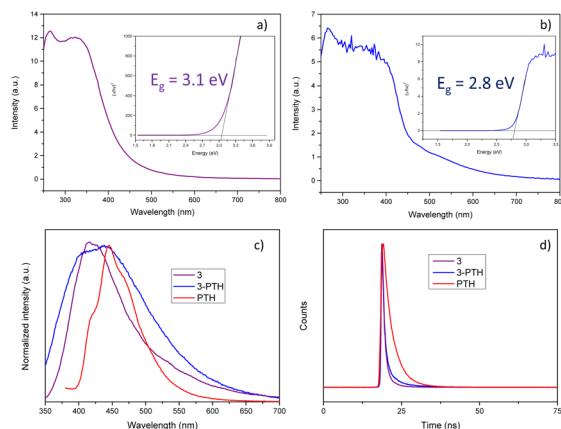


Fig. 3 Results on the photoelectron spectroscopies of samples 3 and 3-PTH. (a) C 1s XPS core level region of sample 3; (b) C 1s XPS core level region of sample 3-PTH; (c) N 1s XPS core level region of sample 3-PTH (inset: XPS N 1s core level region of sample 3); (d) UPS spectra of samples 3 and PTH (inset: edge magnification for valence band determination).

prevents any kind of further analysis. Conversely, the pristine material 3 was silent in these regions due to the lack of PTH units. Finally, the UV Photoelectron Spectroscopy (UPS) data were also recorded for both samples using the HeI line as the excitation source (Fig. 3d). On the one hand, the edge of the valence band was spotted 2.3 eV below the Fermi level for sample 3 and 2.0 eV below the Fermi level for sample 3-PTH. On the other hand, the analysis of the levels afforded a different work function for the materials, since the value for sample 3-PTH, 5.5 eV, was found to be 1.0 eV higher than the value estimated for sample 3 (4.5 eV). This result may be explained by the doping performed by the PTH motif to the structure of the polymer, when functionalized, PTH has been reported previously as a donor moiety able to inject charge into the structure of the host material,<sup>37</sup> as also observed in the optical behavior (see below). Therefore, some sort of conjugation between the PTH motif and the polymer skeleton might be created, maybe as a consequence of the p character of cyclobutane,<sup>44</sup> that facilitates the creation of new levels which justify the electronic properties of material 3-PTH.

The optical properties of the polymers were analyzed employing UV-vis Diffuse Reflectance Spectroscopy (DRS) (Fig. 4). Hence, sample 3 exhibited limited interaction with visible light since no absorption edge was observed until ca. 450 nm where the reflectance started to diminish until saturation. Sample 3-PTH showed similar behavior, with a broader absorption ranged in the visible region. The construction of the Tauc plot using the Kubelka–Munk approach for optical band gap determination afforded values of ~2.8 eV for the functionalized sample 3-PTH and ~3.1 eV for the pristine 3 polymer (insets of Fig. 4), which is a huge contraction and a deep modification of the band structure of the material considering the tiny amount of PTH as a result of the truncation, in agreement with the modifications observed in the work function





**Fig. 4** UV-vis absorption and emission spectroscopy results. Upper panels: Kubelka–Munk transformed absorption and Tauc plot data for samples (a) **3** and (b) **3-PTH**. Lower panels: (c) Normalized emission spectra of pristine **3** and **3-PTH** materials and homogeneous **PTH** in acetonitrile at  $\lambda_{\text{ex}} = 330$  nm. (d) Time-resolved PL decays of pristine **3** and **3-PTH** materials and homogeneous **PTH**. Experiments conducted in degassed acetonitrile with a 375 nm laser.

values. In addition, the band gap energies are comparable to other organic polymers reported previously either conjugated or connected by non-conjugated linkers.<sup>45</sup> Employing the position of the valence band determined with the help of the UPS data and fit, we can locate the energetic levels of our samples as follows: sample **3** would present the valence band at  $-6.8$  eV vs. vacuum ( $E_{\text{vac}}$ ) and with its optical band gap, and the conduction band was found at  $-3.7$  eV vs.  $E_{\text{vac}}$ . In contrast, the donor character of **PTH** may raise the valence band of sample **3-PTH** to  $-6.5$  eV vs.  $E_{\text{vac}}$ , finding, with the help of the optical band gap, the conduction band at  $-3.7$  eV vs.  $E_{\text{vac}}$  (Fig. S12 in the ESI†). Other organic materials previously reported presented comparable band energies.<sup>46</sup>

To further explore the photophysical properties of the materials **3-PTH** and pristine **3**, photoluminescence (PL) experiments and time-resolved fluorescence spectroscopy were performed. The primary conclusion drawn from various emission experiments (Fig. S2 in the ESI†) is that the truncated material **3-PTH** exhibits a lower emission intensity compared to pristine **3**, suggesting an effective reduction in the recombination pathway of the photo-generated electron-hole pairs. In addition, the emission spectrum of material **3-PTH** shows a broad band with two shoulders, which could be ascribed to the maximum emission wavelength of the pristine **3** core and **PTH** moiety at 415 and 447 nm, respectively (Fig. 4c). The time-resolved PL profiles of degassed solutions of **PTH** and suspensions of materials **3-PTH** and pristine **3** in acetonitrile were obtained (Fig. 4d). In the three samples, the decay curves were well fitted using triexponential kinetics, with the first two lifetime components contributing the most (Table 2). The average lifetimes ( $\tau_{\text{avg}}$ ) were calculated to be 3.23 and 3.0 ns for **PTH** and material **3-PTH**, respectively and 1.54 ns for material **3**. These lifetime studies reveal that the excited state of material **3-PTH** exhibited a longer lifetime compared to that of pristine **3**, which

**Table 2** Fluorescence lifetimes ( $\tau_{\text{F}}$ ) of **PTH** and materials **3-PTH** and **3**; charge separation rate constant ( $k_{\text{CS}}$ ) and quantum yield ( $\Phi_{\text{CS}}$ ) of the material **3-PTH**<sup>a</sup>

Sample	$\tau_{\text{F}}$ , ns (%)	$\tau_{\text{avg}}$ , ns (%)	$k_{\text{CS}}$ , s <sup>-1</sup>	$\Phi_{\text{CS}}$
Molecular <b>PTH</b>	1.79 (18)	3.23	—	—
	3.26 (79)			
	12.32 (3)			
Material <b>3-PTH</b>	0.72 (49)	3.0	$8.3 \times 10^8$	0.60
	2.82 (36)		$4.8 \times 10^7$	0.13
	11.21 (15)		$8.0 \times 10^6$	0.09
	—		—	—
Material <b>3</b>	0.76 (72)	1.54	—	—
	2.25 (25)			
	13.14 (3)			

<sup>a</sup>  $\tau_{\text{avg}}$  calculated using the relative amplitudes of the decay components;  $k_{\text{CS}} = 1/\tau_{\text{F}}(\text{material}) - 1/\tau_{\text{F}}(\text{PTH})$ ;  $\Phi_{\text{CS}} = k_{\text{CS}} \times \tau_{\text{F}}(\text{material})$ .

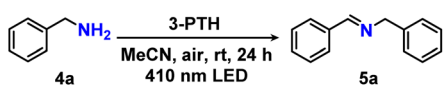
can explain the superior photocatalytic performance exhibited by **3-PTH** (see below). Moreover, the charge-separation rate constants ( $k_{\text{CS}}$ ) and quantum yields ( $\Phi_{\text{CS}}$ ) for the **3-PTH** sample were calculated using **PTH** lifetime data as a reference (Table 2). These values suggested that an efficient charge separation had occurred within **3-PTH**, that together with longer lifetimes would account for the higher reaction rates and more efficient photocatalytic activity of this material (see below).

### Catalytic activity

The photocatalytic activity of the [2 + 2] photocycloaddition polymers, both pristine and truncated, was tested in visible light driven oxidative homocoupling of benzylamines to the corresponding *N*-benzylidene-benzylamine. Thus, we attempted the oxidation of benzylamine **4a** under an air atmosphere in acetonitrile, using 410 nm LED light irradiation according to the analyzed spectral features (Table 3). Under this set of experimental conditions, **3-PTH** was able to promote the oxidation of benzylamine **4a** with a 75% yield in 24 hours (Table 3, entry 1). The analysis of the reaction crude showed the starting material, the product **5a** and less than 1% of byproducts such as aldehydes (see Fig. S13 in the ESI†), demonstrating the high selectivity of this truncated polymer as a photocatalyst. Conversely, pristine polymer **3** struggled in the oxidation of this substrate, achieving 45% yield after the same time of illumination (Table 3, entry 2). Interestingly, we observed decomposition of this pristine material **3** after the reaction, while the truncated polymer **3-PTH** was fully recovered after the experiment (see below). More control experiments were performed with the other truncated samples **3-CN** and **3-CF<sub>3</sub>**, achieving similar results (70% yield and 51% yield, respectively, see Table 3, entry 3 and 4). In addition, the reaction barely presented any background reactivity in the absence of catalyst (Table 3, entry 5). In contrast, the reaction needed light to proceed since a non-illuminated run resulted in negligible conversion (Table 3, entry 6). The reactivity of the heterogeneous catalysts was compared with that of the homogeneous compounds **2-PTH** and **2-ch**. Indeed, the photooxidation of substrate **4a** carried out by using **2-PTH** afforded 60% yield, while the same reaction using the



Table 3 Model oxidative photocoupling of benzyl amines studied<sup>a</sup>

		
Entry	Variation	Yield <sup>b</sup> (%)
1	No variation	75
2	Catalyst = 3	45
3	Catalyst = 3-CN	70
4	Catalyst = 3-CF <sub>3</sub>	51
5	No catalyst	9
6	No light	n.r.
7	Catalyst = 2-PTH	60
8	Catalyst = 2cb	61
9	LED = 385 nm	54
10	LED = 465 nm	24
11	LED = 520 nm	17
12	LED = white	45
13	Solvent = MeOH	31
14	Solvent = 2-ProH	36
15	Solvent = MeOH/H <sub>2</sub> O 1 : 1	45
16	Solvent = DMF	94 <sup>c</sup>
17	Solvent = DCM	38
18	Inert atmosphere	n.r.

<sup>a</sup> Reaction conditions: substrate **4a** (0.2 mmol), 2 mg of heterogeneous catalyst in MeCN (2 mL) under an air atmosphere was irradiated with a 410 nm LED for 24 h at rt. The homogeneous **2-PTH** and **2-cb** loading was 0.3 mol%. <sup>b</sup> Yield (%) determined by <sup>1</sup>H-NMR using 1,3,5-trimethoxybenzene as the internal standard; n.r. stands for *no reaction*. <sup>c</sup> Catalyst decomposition after the reaction.

cyclobutane reference **2-cb** produced 61% yield (Table 3, entries 7 and 8, respectively). Thus, a similar behaviour is shown by the homogeneous photocatalysts in the coupling of benzylamines, even considering the different electronic properties of the monomer and dimer. Nevertheless, heterogenization through the light mediated [2 + 2] polymerization protocol produced an enhancement in the photocatalytic properties of the moiety. After the comparison, we screened the reaction conditions changing the light and the solvent. Indeed, the conversion achieved by **3-PTH** suffered a decay when less energetic LEDs were used because of the misalignment with the absorption maximum (Table 3, entries 10–12), while the use of more energetic light resulted in the formation of more byproducts and consequently in a decrease in yield (entry 9). Therefore, the best illumination source corresponded to the initial blue-purple LED (the comparison with the blank activity is found in Table S1 in the ESI†). Then, the solvent effect was also evaluated (Table 3, entries 13–17), with the best result achieved in acetonitrile despite the high 94% yield achieved in DMF. However, the reaction in DMF provoked a full material etch. In other solvents, such as alcohols or water, the yield was found to be quite lower (17–45%). Finally, molecular oxygen was determined to have a primary role in this photo-oxidation since a catalytic test employing an inert atmosphere (Table 3, entry 16) resulted in negligible conversion.

We also analyzed the temporal evolution of the oxidative visible light homocoupling of benzylamines by withdrawing

aliquots from the reaction, using **4a** as the substrate in acetonitrile in air (Fig. 5a). Interestingly, after turning on the LED, the yield linearly increased in the first 7 hours of irradiation, achieving a value of around 60%. Then, the rate of the reaction slowed down until achieving a steady state close to a plateau at 72% yield after 16 h. Letting the reaction run for longer times, *i.e.*, 24 h of illumination, allowed the yield to reach the previously discussed 75% value. This catalytic behaviour was observed to be completely different from the background reaction, whose conversion values slowly but constantly increased until 9% yield. Interestingly, the catalytic performance showed by sample **3** was found to be inferior compared to the activity observed for sample **3-PTH**, as predicted by the band alignment and optical behaviour discussed above. Conversely, the activity observed for the homogeneous reference **2-PTH** followed a similar kinetic scenario but achieving less activity than the best sample in this study, sample **3-PTH**. Indeed, it showed similar catalytic activity to other state-of-the-art catalysts reported before for this particular photochemical transformation (see benchmark in Table S3 in the ESI†).

Based on these kinetic points, the stability and robustness of the material was evaluated. On the one hand, we subjected sample **3-PTH** to consecutive recovery and reaction cycles (Fig. 5b). Once the reaction reached the steady state region of the kinetic profile (24 h of illumination), we recovered the catalyst by centrifugation methods, and it was profusely washed with fresh dichloromethane and acetone to remove any remaining impurity. Next, we performed another photocatalytic test without adding any new catalyst precursor. We let the photooxidative coupling reaction of substrate **4a** run for 24 h and we analyzed the conversion. The procedure was repeated 4 times, and only a small loss of conversion was observed in the last run. In contrast, sample **3** exhibited a progressive loss of

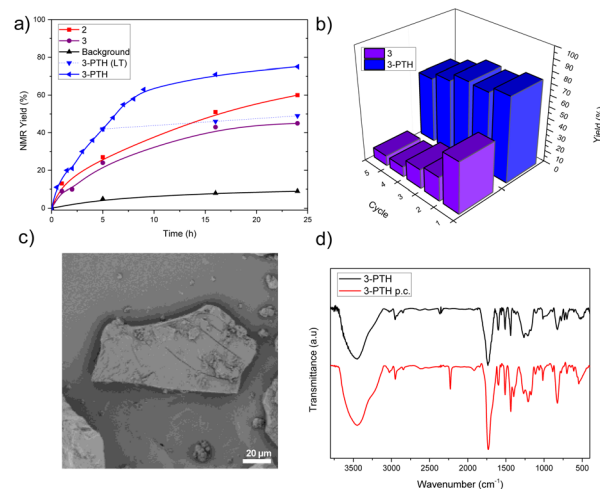


Fig. 5 (a) Temporal evolution of the light-driven oxidative coupling of benzylamine **4a** catalyzed by the samples under study (yield was determined by <sup>1</sup>H-NMR using 1,3,5-trimethoxybenzene as the internal standard). (b) Recovery study of sample **3-PTH** and **3** in the coupling of substrate **4a**. (c) SEM analysis of sample **3-PTH** recovered after 5 catalytic cycles. (d) FT-IR of sample **3-PTH** recovered after 5 catalytic cycles (red line).

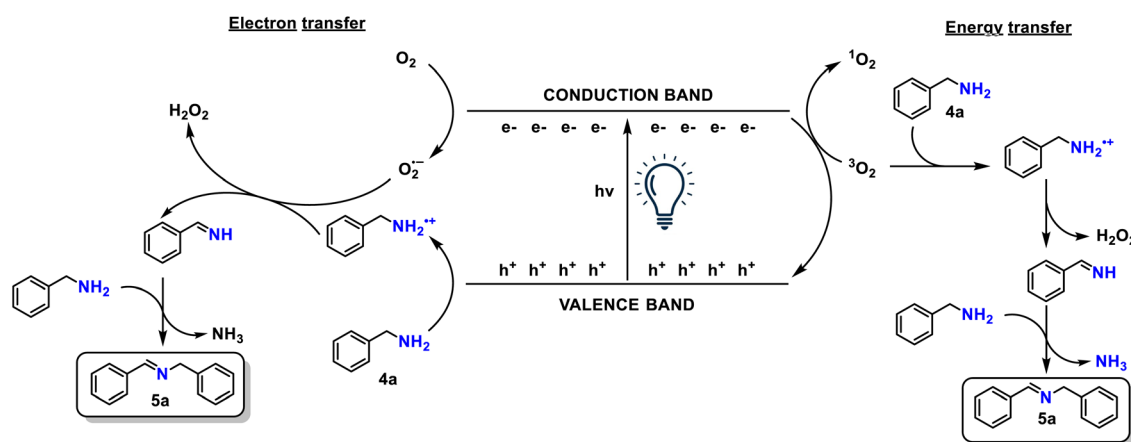


activity during the recovery procedure. We observed that the amount of polymer **3** recovered diminished after each run, which may be a symptom of instability of the material during operation that consumes the polymer. This was not observed for sample **3-PTH**, which was robust enough for not leaching any material to the reaction medium, as demonstrated by a “hot filtration” experiment in the coupling of substrate **4a** (Fig. 5a LT trace).<sup>37,47</sup> After removing the catalyst from the reaction by filtration at yields of around 50% (*i.e.* 6 h) and illuminating the filtrate again, no increment in the conversion was observed, as an indication of the absence of active species leached out into the reaction medium (see the homogeneous catalyst test for comparison in Table 2). This test highlights the stability of the truncated polymer **3-PTH** as a photocatalyst for organic transformations.

After assessing the temporal performance and stability of the catalyst, we wanted to get insights into the reaction mechanism. To do this, we conducted different photocatalytic oxidative couplings of benzylamine **4a** by varying the conditions and adding scavengers of intermediates reported to have a role in the mechanism of the reaction,<sup>48,49</sup> allowing us to make the proposal illustrated in Scheme 4. In particular, we tested the role of singlet oxygen, superoxide species, hydrogen peroxide and hydroxyl radicals (see Table S2 in the ESI†), analyzing the yield by NMR after each experiment. As stated above, the reaction needs oxygen to proceed, highlighting its role as the oxidant of this transformation. This oxygen can be slightly converted to singlet oxygen since the quenching experiment with DABCO afforded 66% conversion (Scheme 4 right path). Thus, this highly reactive species shall react with substrate **4a** to produce an imine intermediate. Nevertheless, the high conversion observed in the experiment of the singlet oxygen quenching may indicate that the electron transfer mechanism seems more plausible. In this situation (Scheme 4 left path), the illumination should produce the excitation of the material that yields the oxidation of the amine **4a**. As a result of these redox reactions, the iminic intermediate and hydrogen peroxide are obtained, possibly through the formation of superoxide intermediate species (the quenching with *p*-benzoquinone resulted

in 47% conversion, see Table S2 in the ESI†). At this point, another molecule of substrate **4a** can perform a nucleophilic attack on the imine, and after ammonia elimination, product **5a** can be generated. The reaction cycle was closed by the decomposition of  $\text{H}_2\text{O}_2$  into a hydroxy radical, which was important for the cycle (a reaction with *tert*-butyl alcohol ( $\text{OH}^\cdot$  scavenger), resulting in 16% yield, see Table S2†). Finally, as indicated above, molecular oxygen was important too as a substrate for catalyst **3-PTH**, because an oxidative coupling of **4a** performed in pure  $\text{O}_2$  resulted in 71% yield, confirming the role of oxygen and hydrogen peroxide and the versatility of catalyst **3-PTH** in this model reaction.

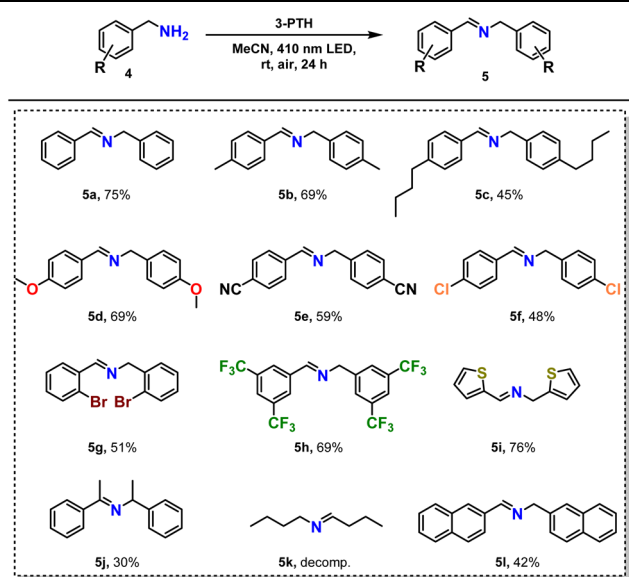
We also evaluated the scope of the reaction by changing the nature of the substrate subjected to the photooxidative coupling. The results are depicted in Table 4. On the one hand, model substrate **4a** could be converted to the corresponding imine **5a** in a good 75% yield, as previously stated. This outcome was not modified by adding a methyl group at the *para* position of the benzene ring, since substrate **4b** could be converted with a similar yield (69% yield). However, the steric requirements of the alkyl chains present in substrate **4c** made the synthesis of imine **5c** proceed in a lower 45% yield. Interestingly, catalyst **3-PTH** could proceed with the oxidative photocoupling regardless of the electronic nature of the substrate. For instance, electron donor moieties as a *p*-methoxy group at the benzene ring (substrate **4d**) resulted in an oxidation with 69% yield, while the yield was not significantly decreased using an electron withdrawing group as the *p*-cyano substituent (yield of **5e** = 59%). Halogens were also tolerated regardless of their relative position, because the oxidations of **4f** (*p*-chloro group, 48% yield) and **4g** (*o*-bromo group, 51% yield) were performed with similar results. In addition, a difunctionalized benzylamine at *meta* positions with trifluoromethyl groups (substrate **4h**) was also oxidized with a good performance of 69% yield. Interestingly, heterocycles could be also coupled since the synthesis of thiophenyl imine **5i** was performed with a very good 76% yield. We also attempted the oxidative coupling of more challenging substrates. On the one hand,  $\alpha$ -alkylated imine **5j** was obtained in 30% yield, while an aliphatic substrate such as butylamine **4k** resulted in the



Scheme 4 Proposed reaction mechanism according to quenching studies.





**Table 4** Scope of the benzylamine light-driven coupling catalyzed by 3-PTH<sup>a</sup>

<sup>a</sup> Reaction conditions: substrate **4** (0.2 mmol) and 8 mg of **3-PTH** in MeCN (2 mL) under an air atmosphere was irradiated under 410 nm LED for 24 h at rt. Values stand for yield (%) determined by <sup>1</sup>H-NMR using 1,3,5-trimethoxybenzene as the internal standard.

decomposition of the product. Furthermore, polycyclic 2-naphthylmethylamine **4l** was converted to the corresponding imine in a 42% yield. In this later case 33% of 2-naphthaldehyde was observed as a byproduct in the reaction crude.

## Experimental section

### General information. Materials and methods

All chemicals, solvents and reagents were purchased from commercial sources (reagent grade quality or better) and used without further purification if not otherwise stated. The aryl amines used for the catalytic photooxidation tests were purified *via* distillation when needed. Purification of organic products, when necessary, was accomplished by flash chromatography using silica gel (Merck Geduran® Si 60) in an adequate mixture of cyclohexane (CyH) and ethyl acetate (EtOAc) eluents. The synthesis of monomers **1**, **2-PTH**, **2-cb**, **2-CN** and **2-CF<sub>3</sub>** was adapted from literature procedures<sup>35,37</sup> and is fully described in the ESI.† All the organic products were characterized by comparison of their <sup>1</sup>H nuclear magnetic resonance (NMR) spectral data with those reported in the literature or from commercial sources. In the case of new compounds, <sup>1</sup>H NMR, <sup>13</sup>C NMR and mass spectrometry (MS) spectra were recorded and presented in the ESI.† Characterization methods are also fully described in the ESI.†

### Light-driven [2 + 2] synthesis of polymers

The typical synthesis of the organic extended materials was performed, if not otherwise stated, as follows: a vial was charged

with a magnetic stirring bar, the organic monomer **1** (0.2 mmol) and the solvent (acetonitrile, MeCN) (2 mL). The vial was sealed and placed under an inert atmosphere performing 3 consecutive degassing 3 freeze–pump–thaw cycles and irradiated with a 385 nm LED at room temperature for the desired time, typically 40 h. After that time, the vial was opened and a solid was formed at the bottom of the vial, which was profusely washed by 5 centrifugation cycles with 15 mL of fresh dichloromethane (DCM) each time. Drying in an oven at 60 °C for 16 h afforded the final polymer **3**. The synthesis of the truncated systems **3-CN**, **3-CF<sub>3</sub>** and **3-PTH** was performed identically but adding 0.02 mmol of molecule **2-CN**, **2-CF<sub>3</sub>** or **2-PTH** to the reaction vial.

### Photocatalytic oxidative benzylamine homocoupling

The typical catalytic test based on the benzyl amine light-driven oxidative coupling was performed, if not otherwise stated, as follows:<sup>50</sup> a vial was charged with a magnetic stirring bar, the amine **4a–l** (0.2 mmol), the catalyst (2–8 mg of the [2 + 2] photocycloaddition polymers or 0.3 mol% of the homogeneous catalysts) and the solvent (MeCN, 2 mL). The vial was sealed and irradiated with a 410 nm LED while stirring at room temperature for the desired time, typically 24 h. 0.05–0.1 mL aliquots were periodically withdrawn from the reaction vessel to track the progress of the reaction through analysis by <sup>1</sup>H-NMR spectroscopy. The yields were calculated by <sup>1</sup>H-NMR using 1,3,5-trimethoxybenzene as the internal standard. The full experimental details for each imine **5** and their characterization data are described in the ESI.†

### Catalyst recovery, recycling and leaching

After the reaction was considered completed, the polymeric photocatalysts were recovered by filtration through polytetrafluoroethylene (PTFE) membranes and then washed 3 times with acetone and 3 further times with DCM, and the solid was finally vacuum-dried. Following this procedure, the heterogeneous catalyst was employed in a new catalytic cycle by adding all the reagents and solvents. This procedure was repeated several times, analyzing the outcome of the reaction by the <sup>1</sup>H-NMR method. The eventual leaching was monitored by means of a “hot-filtration” experiment. To perform this task, the coupling of benzylamine **4a** using **3-PTH** as the catalyst was allowed to proceed for a desired time, *i.e.* 5 h. The reaction was removed from light, the heterogeneous catalyst was filtered off, and the reaction solution was returned to under the LED for further illumination (additional 16 h and 24 h). The filtrate mixture was monitored by withdrawing aliquots at regular intervals and analyzing them by <sup>1</sup>H-NMR spectroscopy.

## Conclusions

This work describes the employment of olefin [2 + 2] photocycloaddition as a tool for the construction of a covalent organic polymer, yielding the material **3**. The material characterization showed the establishment of cyclobutane moieties as linkages among the monomers as a result of the proposed light-driven methodology. In addition, this photopolymerization was



compatible with the monomer truncation strategy to expand the functionality of the system. Indeed, nitrile **3-CN**, trifluoromethyl **3-CF<sub>3</sub>** and 10-phenyl-phenothiazine **3-PTH** truncated polymers were prepared under UV-light irradiation with a functionalization degree of 10 mol%. According to the photophysical study, truncate material **3-PTH** improved the photophysical properties of pristine **3**, by lowering the recombination of the photo-generated electrons and holes and exhibiting longer excited state lifetime. Moreover, the truncation with a photoactive moiety boosted the photocatalytic activity and increased the robustness of the **3-PTH** sample under specific reaction conditions compared to the other materials in this study. Hence, **3-PTH** accounted for higher yield levels and recyclability without degradation or leaching. It also exhibited wide scope towards 19 different amines, with yields ranging 30–75% under the conditions evaluated. As a whole, we believe that this method paves the way for new reactivities for the construction of covalent organic polymers under light irradiation with advanced applications beyond conventional polar synthetic methods, demonstrating at the same time that the novel methodology is compatible with the monomer truncation strategy to increase the functionality of the obtained systems.

## Data availability

The data supporting this article have been included as part of the ESI.†

## Conflicts of interest

There are no conflicts to declare.

## Acknowledgements

This work was supported by MICINN (PID2021-122299NB-I00, TED2021-129999B-C32, and TED2021-130470B-I00), “Comunidad de Madrid” for European Structural Funds (S2018/NMT-4367) and proyectos sinérgicos I+D (Y2020/NMT-6469).

## Notes and references

- R. Freund, S. Canossa, S. M. Cohen, W. Yan, H. Deng, V. Guillerm, M. Eddaoudi, D. G. Madden, D. Fairen-Jimenez, H. Lyu, L. K. Macreadie, Z. Ji, Y. Zhang, B. Wang, F. Haase, C. Wöll, O. Zaremba, J. Andreo, S. Wuttke and C. S. Diercks, *Angew. Chem., Int. Ed.*, 2021, **60**, 23946–23974.
- O. M. Yaghi, *ACS Cent. Sci.*, 2019, **5**, 1295–1300.
- H.-C. Zhou and S. Kitagawa, *Chem. Soc. Rev.*, 2014, **43**, 5415–5418.
- T. F. Machado, M. E. S. Serra, D. Murtinho, A. J. M. Valente and M. Naushad, *Polymers*, 2021, **13**, 970.
- X. Sun, M. Di, J. Liu, L. Gao, X. Yan and G. He, *Small*, 2023, **19**, 2303757.
- R. Shah, S. Ali, F. Raziq, S. Ali, P. M. Ismail, S. Shah, R. Iqbal, X. Wu, W. He, X. Zu, A. Zada, A. F. Mabood, A. Vinu, S. H. Jhung, J. Yi and L. Qiao, *Coord. Chem. Rev.*, 2023, **477**, 214968.
- J. Feng, Q.-Y. Huang, C. Zhang, S. Ramakrishna and Y.-B. Dong, *Int. J. Biol. Macromol.*, 2023, **248**, 125729.
- S. Liu, M. Wang, Y. He, Q. Cheng, T. Qian and C. Yan, *Coord. Chem. Rev.*, 2023, **475**, 214882.
- A. López-Magano, S. Daliran, A. R. Oveisi, R. Mas-Ballesté, A. Dhakshinamoorthy, J. Alemán, H. Garcia and R. Luque, *Adv. Mater.*, 2023, **35**, 2209475.
- H. Fan, H. Wang, M. Peng, H. Meng, A. Mundstock, A. Knebel and J. Caro, *ACS Nano*, 2023, **17**, 7584–7594.
- Y. Shi, J. Yang, F. Gao and Q. Zhang, *ACS Nano*, 2023, **17**, 1879–1905.
- W. Huang, W. Zhang, S. Yang, L. Wang and G. Yu, *Small*, 2024, **20**, 2308019.
- A. López-Magano, A. Jiménez-Almarza, J. Alemán and R. Mas-Ballesté, *Catalysts*, 2020, **10**, 720.
- Y. Zhang, G. Lu, D. Zhao and X. Huang, *Mater. Chem. Front.*, 2023, **7**, 4782–4809.
- R. Xue, Y.-S. Liu, S.-L. Huang and G.-Y. Yang, *ACS Sens.*, 2023, **8**, 2124–2148.
- X. Guan, F. Chen, S. Qiu and Q. Fang, *Angew. Chem., Int. Ed.*, 2023, **62**, e202213203.
- X. Feng, X. Ding and D. Jiang, *Chem. Soc. Rev.*, 2012, **41**, 6010–6022.
- A. Giri, Y. Khakre, G. Shreeraj, T. K. Dutta, S. Kundu and A. Patra, *J. Mater. Chem. A*, 2022, **10**, 17077–17121.
- Y. Wang, Y. Yang, Q. Deng, W. Chen, Y. Zhang, Y. Zhou and Z. Zou, *Adv. Funct. Mater.*, 2023, **33**, 2307179.
- J.-Y. Tang and Y. Sun, *Mater. Adv.*, 2020, **1**, 2155–2162.
- P. Bellotti, H.-M. Juang, T. Faber and F. Glorius, *Chem. Rev.*, 2023, **123**, 4237–4352.
- H.-B. Cheng, S. Zhang, E. Bai, X. Cao, J. Wang, J. Qi, J. Liu, J. Zhao, L. Zhang and J. Yoon, *Adv. Mater.*, 2022, **34**, 2108289.
- A. Gellé, T. Jin, L. de la Garza, G. D. Price, L. V. Besteiro and A. Moores, *Chem. Rev.*, 2020, **120**, 986–1041.
- G.-B. Wang, Y.-J. Wang, J.-L. Kan, K.-H. Xie, H.-P. Xu, F. Zhao, M.-C. Wang, Y. Geng and Y.-B. Dong, *J. Am. Chem. Soc.*, 2023, **145**, 4951–4956.
- C.-J. Wu, X.-Y. Li, T.-R. Li, M.-Z. Shao, L.-J. Niu, X.-F. Lu, J.-L. Kan, Y. Geng and Y.-B. Dong, *J. Am. Chem. Soc.*, 2022, **144**, 18750–18755.
- C.-J. Wu, M.-Z. Shao, S. J. Kan, W.-J. Liang, T.-R. Li, L.-J. Niu, N.-H. Wang, Y. Geng and Y.-B. Dong, *ACS Mater. Lett.*, 2024, **6**, 5016–5022.
- S. Poplata, A. Tröster, Y.-Q. Zou and T. Bach, *Chem. Rev.*, 2016, **116**, 9748–9815.
- D. I. Schuster, G. Lem and N. A. Kaprinidis, *Chem. Rev.*, 1993, **93**, 3–22.
- M. Sicignano, R. I. Rodríguez and J. Alemán, *Eur. J. Org. Chem.*, 2021, **2021**, 3303–3321.
- R. Medishetty, I.-H. Park, S. S. Lee and J. J. Vittal, *Chem. Commun.*, 2016, **52**, 3959–4001.
- B. B. Rath and J. J. Vittal, *J. Am. Chem. Soc.*, 2020, **142**, 20117–20123.
- A. López-Magano, A. E. Platero-Prats, S. Cabrera, R. Mas-Ballesté and J. Alemán, *Appl. Catal., B*, 2020, **272**, 119027.
- D. N. Bunck and W. R. Dichtel, *Angew. Chem., Int. Ed.*, 2012, **51**, 1885–1889.



- 34 S. Daliran, M. Blanco, A. Dhakshinamoorthy, A. R. Oveisi, J. Alemán and H. García, *Adv. Funct. Mater.*, 2024, **34**, 2312912.
- 35 M. Zhao, S. Ou and C.-D. Wu, *Cryst. Growth Des.*, 2017, **17**, 2688–2693.
- 36 T. Ai, Y. Xu, L. Qiu, R. J. Geraghty and L. Chen, *J. Med. Chem.*, 2015, **58**, 785–800.
- 37 J. L. Nova-Fernández, D. González-Muñoz, G. Pascual-Coca, M. Cattelan, S. Agnoli, R. Pérez-Ruiz, J. Alemán, S. Cabrera and M. Blanco, *Adv. Funct. Mater.*, 2024, **34**, 2313102.
- 38 S. O. Poelma, G. L. Burnett, E. H. Discekici, K. M. Mattson, N. J. Treat, Y. Luo, Z. M. Hudson, S. L. Shankel, P. G. Clark, J. W. Kramer, C. J. Hawker and J. Read De Alaniz, *J. Org. Chem.*, 2016, **81**, 7155–7160.
- 39 L. Djakovitch and K. Koehler, *J. Am. Chem. Soc.*, 2001, **123**, 5990–5999.
- 40 J. Datka and E. Kukulska-Zajac, *J. Phys. Chem. B*, 2004, **108**, 17760–17766.
- 41 K. Ruhland, R. Frenzel, R. Horny, A. Nizamutdinova, L. van Wüllen, J. Moosburger-Will and S. Horn, *Polym. Degrad. Stab.*, 2017, **146**, 298–316.
- 42 E. D. Glendening and A. M. Halpern, *J. Phys. Chem. A*, 2005, **109**, 635–642.
- 43 M. Sciarretta, M. Barawi, C. Navío, V. A. P. O'Shea, M. Blanco and J. Alemán, *ACS Appl. Mater. Interfaces*, 2022, **14**, 34975–34984.
- 44 M. R. Van der Kolk, M. A. C. H. Janssen, F. P. J. T. Rutjes and D. Blanco-Ania, *ChemMedChem*, 2022, **17**, e202200020.
- 45 S. Gao, P. Zhang, G. Huang, Q. Chen, J. Bi and L. Wu, *ChemSusChem*, 2021, **14**, 3850–3857.
- 46 N. Singh, D. Yadav, S. V. Mulay, J. Y. Kim, N.-J. Park and J.-O. Baeg, *ACS Appl. Mater. Interfaces*, 2021, **13**, 14122–14131.
- 47 D. González-Muñoz, J. Alemán, M. Blanco and S. Cabrera, *J. Catal.*, 2022, **413**, 274–283.
- 48 A. Das, K. R. J. Mohit and K. R. J. Thomas, *J. Org. Chem.*, 2023, **88**, 14065–14077.
- 49 T. Mitkina, C. Stanglmair, W. Setzer, M. Gruber, H. Kisch and B. König, *Org. Biomol. Chem.*, 2012, **10**, 3556–3561.
- 50 A. Jiménez-Almarza, A. López-Magano, R. Mas-Ballesté and J. Alemán, *ACS Appl. Mater. Interfaces*, 2022, **14**, 16258–16268.

